

Bacterial community dynamics on bats and the implications for pathogen resistance

Aoqiang Li,^{1,2} Zhongle Li,^{1,3} Wentao Dai,¹ Katy L. Parise,⁴ Haixia Leng,¹ Longru Jin,¹ Sen Liu,⁵ Keping Sun ¹, ^{1*} Joseph R. Hoyt^{6*} and Jiang Feng^{1,7} Jilin Provincial Key Laboratory of Animal Resource Conservation and Utilization, Northeast Normal University, 2555 Jingyue Street, Changchun, 130117, China.

²Key Laboratory of Vegetation Ecology, Ministry of Education, Changchun, 130024, China.

³College of Animal Science and Technology, Jilin Agricultural University, Changchun, 130118, China.

⁴Pathogen and Microbiome Institute, Northern Arizona University, Flagstaff, AZ, 86011.

⁵College of Life Sciences, Henan Normal University, Xinxiang, 453007, China.

⁶Department of Biological Sciences, Virginia Polytechnic Institute, Blacksburg, VA, 24060.

⁷College of Life Science, Jilin Agricultural University, Changchun, 130118, China.

Summary

The bats skin microbiota plays an important role in reducing pathogen infection, including the deadly fungal pathogen Pseudogymnoascus destructans, the causative agent of white-nose syndrome. However, the dynamic of skin bacterial communities response to environmental perturbations remains poorly described. We characterized skin bacterial community over time and space in Rhinolophus ferrumequinum, a species with high resistance to the infection with P. destructans. We collected environmental covariate data to determine what factors influenced changes in community structure. We observed significant temporal and spatial shifts in the skin bacterial community, which was mainly associated with variation in operational taxonomic units. The skin bacterial community differed by the environmental microbial reservoirs and was most

Received 19 March, 2021; revised 7 July, 2021; accepted 30 August, 2021. *For correspondence. E-mail sunkp129@nenu.edu.cn; Tel. 0431-89165610. E-mail hoytjosephr@gmail.com; Tel. (518) 965-7120.

influenced by host body condition, bat roosting temperature and geographic distance between sites, but was not influenced by pathogen infection. Furthermore, the skin microbiota was enriched in particular taxa with antifungal abilities, such as Enterococcus, Burkholderia, Flavobacterium, Pseudomonas, Corynebacterium and Rhodococcus. And specific strains of Pseudomonas, Corynebacterium and Rhodococcus even inhibited P. destructans growth. Our findings provide new insights in characterizing the variation in bacterial communities can inform us about the processes of driving community assembly and predict the host's ability to resist or survive pathogen infection.

Introduction

Microbial communities can form a symbiotic or commensal relationship with their hosts and play an essential role in protection from invading pathogens (Round and Mazmanian, 2009; Grice and Segre, 2011; Thaiss et al., 2016). The host-associated microbial communities can be influenced by a myriad of factors including environmental conditions (Pantos et al., 2015), environmental microbial reservoirs (Loudon et al., 2014), host body condition (Hernández-Gómez et al., 2018) and pathogen infection (Byrd et al., 2018), which can vary over time and among populations. Although the stability of microbial communities to various stressors has been documented (Azarbad et al., 2016; Oh et al., 2016), few studies have explored the influence of multiple abiotic and biotic factors on microbial community structure and composition.

The recent introduction of the fungus *Pseudo-gymnoascus destructans*, which causes white-nose syndrome (WNS), to North America has resulted in devastating impacts to bat populations (Lorch *et al.*, 2011; Langwig *et al.*, 2012; Langwig *et al.*, 2016; Drees *et al.*, 2017). During pathogen infection, host-associated bacterial communities could be an important factor in WNS disease dynamics, as they can provide a benefit to their host against pathogen infection and have been previously shown to increase bat survival both *in vitro* (Hoyt *et al.*, 2015; Micalizzi *et al.*, 2017) and *in*

situ (Hovt et al., 2019). Limited data on the skin microbiota in relation to WNS have been reported (Lemieux-Labonté et al., 2017; Ange-Stark et al., 2019; Grisnik et al., 2020), particularly for bats with high resistance to P. destructans in the endemic region, such as in Asia. Considering that bat skin bacterial communities are vulnerable to external stressors, especially during hibernation when skin may be in direct contact with local environment for long periods of time (Hoyt et al., 2018), assessing temporal and spatial dynamics of hostassociated microbial communities is crucial for understanding and forecasting their response to environment change and pathogen infection, and ultimately affecting their defensive function against pathogens. For instance, amphibian skin microbiota exhibited the temporal and spatial changes primarily caused by phylogenetic constraints, microbiota reservoirs, environmental temperature or fungal infection, which may eventually affect host health (e.g. Walke and Belden, 2016; Jiménez and Sommer, 2017; Rebollar et al., 2020). However, the complex interactions of how host-associated microbiota are influenced by the environment, pathogen infection, and in turn, their influence on bat host resistance over time and space remains an outstanding question.

Here we examine the variation in skin bacterial communities and what factors most influenced changes in community structure from Rhinolophus ferrumequinum over time and among populations in these communities to an invading fungal pathogen. This is a widespread bat species in China that has been shown to have low fungal loads over winter (Hoyt et al., 2016a; Hoyt et al., 2020). We hypothesized that bat skin bacterial assemblage structure would exhibit both temporal and spatial variability over the hibernation period, and environmental bacterial communities and external conditions, such as temperature, geographic distance among populations, body condition and infection would influence the observed variation. In order to address our hypothesis, we sampled bacterial communities from bats skin and collected environmental covariate data over time and space to characterize the community structure of bat skin and environment.

Results

P. destructans infection status of R. ferrumequinum

Pseudogymnoascus destructans was detected in all but one sampling time point, with bats not testing positive for the fungus at the start of the hibernation season, December. From January to April, the quantity of P. destructans (\log_{10} ng of DNA) was not significantly different among sampling points (average -5.53, -5.87 and -4.93 respectively; Kruskal–Wallis test, P > 0.05;

Fig. S1a). We also detected the presence of P. destructans at all sites during late hibernation. The average log-transformed fungal loads were -3.60, -2.08, -4.85, -3.73 and -4.93 for HN, BJ, JL2, LN and JL1 respectively (Fig. S1b).

Variation of skin bacteria within and among populations

A total of 3408 and 4354 OTUs were identified over four sampling time points and across five sites respectively. Across all samples, the dominant taxa were from four main phyla: Firmicutes, Proteobacteria, Actinobacteria and Bacteroidetes (Fig. S2).

Pairwise comparisons of Shannon diversity between four sampling time points showed no significant differences, except for one comparison between December and January that was significantly different (Wilcox: $P_{\rm adj} < 0.001$; Fig. 1A). The other two alpha diversity indices (Observed OTUs and PD) did not differ significantly over time (Kruskal–Wallis; Observed OTUs, $\chi^2 = 6.68$, P = 0.08; PD, $\chi^2 = 7.01$, P = 0.07; Figs S3a and 3B). Similar results were obtained for Observed OTUs and PD across different sites (Figs S3c and 3D). However, we found significant variation in Shannon diversity between some of the sites (Fig. 1B), that is, LN harboured higher diversity than HN (Wilcox: $P_{\rm adj} < 0.01$) and JL1 (Wilcox: $P_{\rm adj} < 0.001$).

Skin bacterial communities varied over time and among different populations of R. ferrumequinum. Nonmetric multidimensional scaling (NMDS) revealed a clear temporal pattern in which samples were largely partitioned by sampling time points, suggesting community structure varied across all time points, except for between January and February (NMDS with stress = 0.14; PER-MANOVA, Pseudo- $F_{3,62} = 13.08$, P = 0.001, $R^2 = 0.40$; Fig. 1C). Consistently, hierarchical clustering also revealed that the samples from January and February clustered together suggesting bats have similar community structure over this period (Fig. S4). Furthermore, PER-MANOVA also indicated that variability in skin bacterial communities was also observed among sites (NMDS with stress = 0.20; PERMANOVA, Pseudo- $F_{4,63}$ = 5.09, P = 0.001, $R^2 = 0.26$; Fig. 1D). The dispersion values showed significant differences in the distance to the centroid over time, which was driven by the differences between December with the least variation and each other sampling time point (betadisper: $F_{3.59} = 16.19$, P<0.001; Fig. S5). However, there was no significant difference in the dispersion values across sites (betadisper: $F_{4.59} = 1.70$, P = 0.17). In addition, comparison of individuals that tested either positive or negative for P. destructans at a given sampling time point or site showed that the presence of P. destructans on bats did not alter the skin bacterial community structure (Time: PER-MANOVA, Pseudo- $F_{1,62} = 1.78$, P = 0.95, $R^2 = 0.03$;

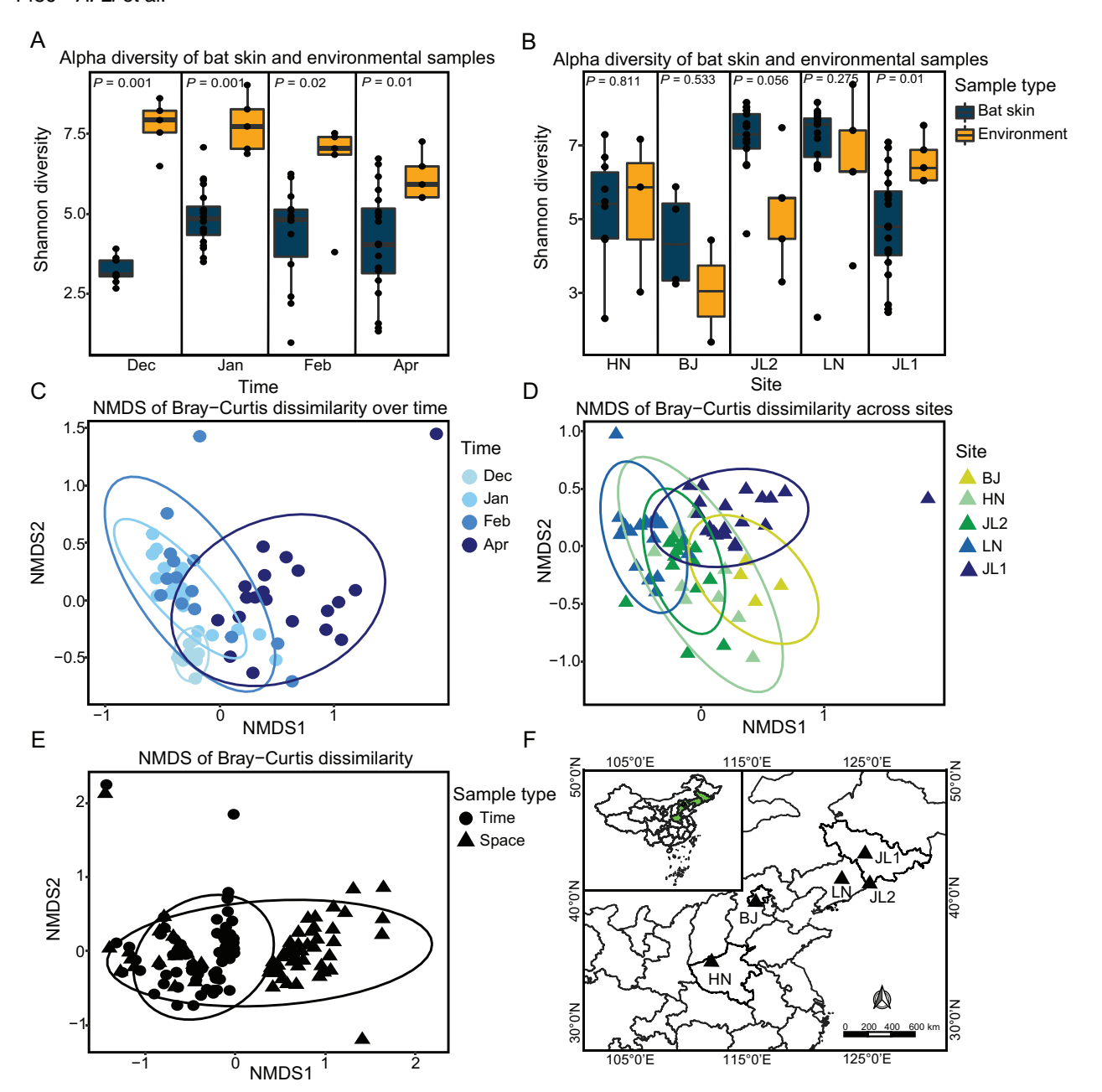


Fig. 1. Temporal and spatial changes of skin bacterial community in *R. ferrumequinum*. Shannon diversity of bat skin and corresponding environmental samples over time (A) and among sites (B). Non-metric multidimensional scaling (NMDS) plots of Beta diversity (Bray–Curtis dissimilarity) among four time points (C), and five sites (D), as well as between time and space (E). Ellipses (C, D and E) represent confidence intervals (Cl) of 95%. (F) Sample localities of *R. ferrumequinum* population used in this study.

Space: PERMANOVA, Pseudo- $F_{1,63}=1.15$, P=0.56, $R^2=0.02$). Contrary to our expectations, male and female bats at each sampling time point or site showed similar bacterial communities (Time: PERMANOVA, Pseudo- $F_{1,62}=1.44$, P=0.094, $R^2=0.02$; Space: PERMANOVA, Pseudo- $F_{1,63}=1.03$, P=0.15, $R^2=0.02$).

After controlling for sampling time points using partial regression analysis, we found that BMI was a significant predictor of Observed OTUs ($F_{(1,59)} = 7.791$, P = 0.007,

Fig. 2A) and PD ($F_{(1,59)} = 7.556$, P = 0.008, Fig. 2B) over four sampling time points, and as bats BMI decreased, observed OTUs and PD also decreased. However, the correlation between BMI and Shannon diversity was not significant ($F_{(1,59)} = 2.912$, P = 0.093, Fig. S6). Those results also showed that a negative but no significant relationship between alpha diversity and bat roosting temperature (all P > 0.05, Figs 2 and S6). Contrary to our expectations, fungal loads had no significant effect on the

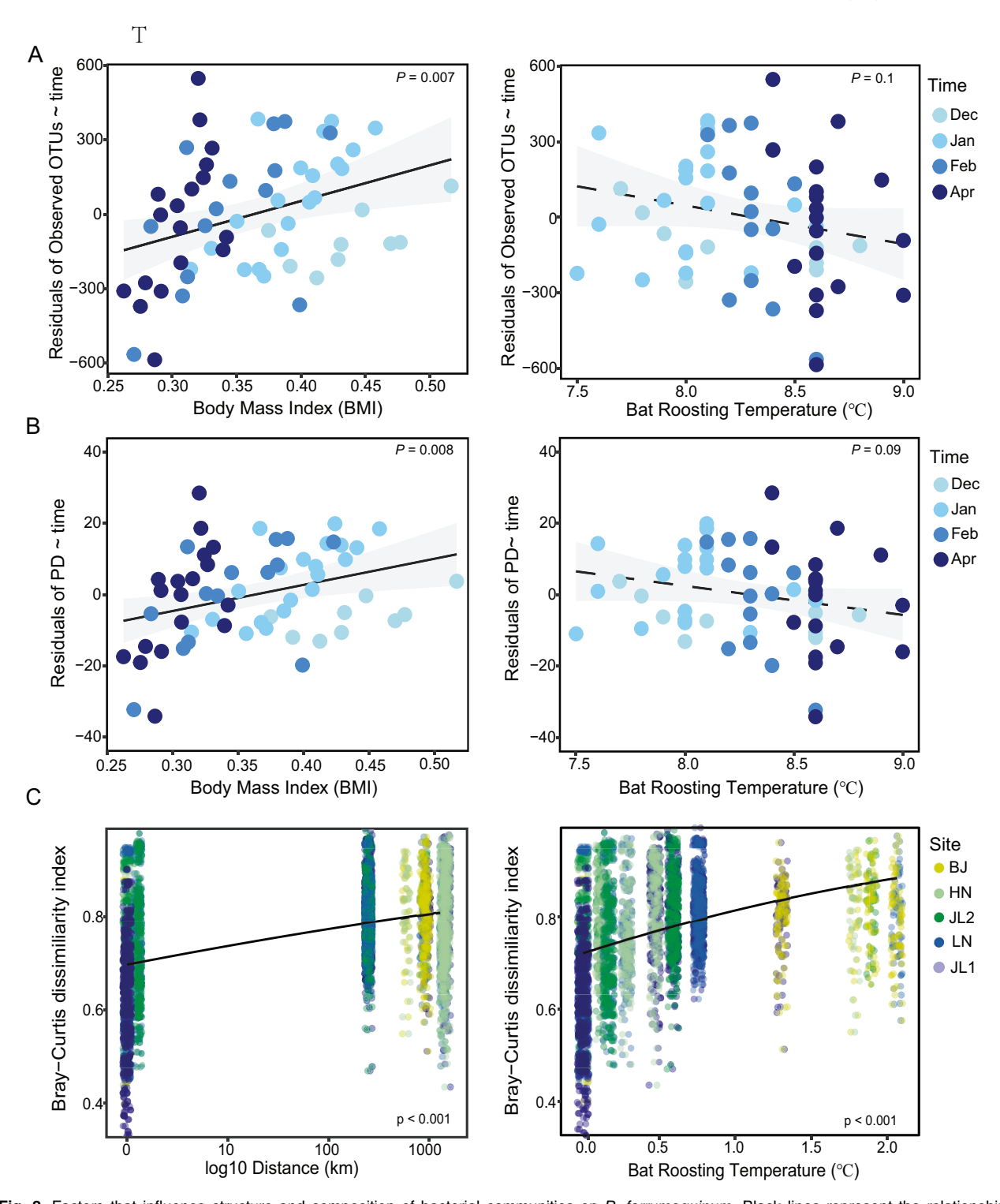


Fig. 2. Factors that influence structure and composition of bacterial communities on *R. ferrumequinum*. Black lines represent the relationship between BMI and alpha diversity is significant. Dashed lines represent the relationship between factors (BMI and bat roosting temperature) and alpha diversity is marginal. Gray ribbons show 95% confidence intervals (CI). (A) and (B) Relationship between alpha diversity of host skin and bat roosting temperature and body mass index in four time points. (C) Effect of geographic distance (on a log₁₀ scale) and bat roosting temperature on Bray–Curtis dissimilarity among individual pairs of bats based on generalized linear mixed model with a beta distribution and a logit link.

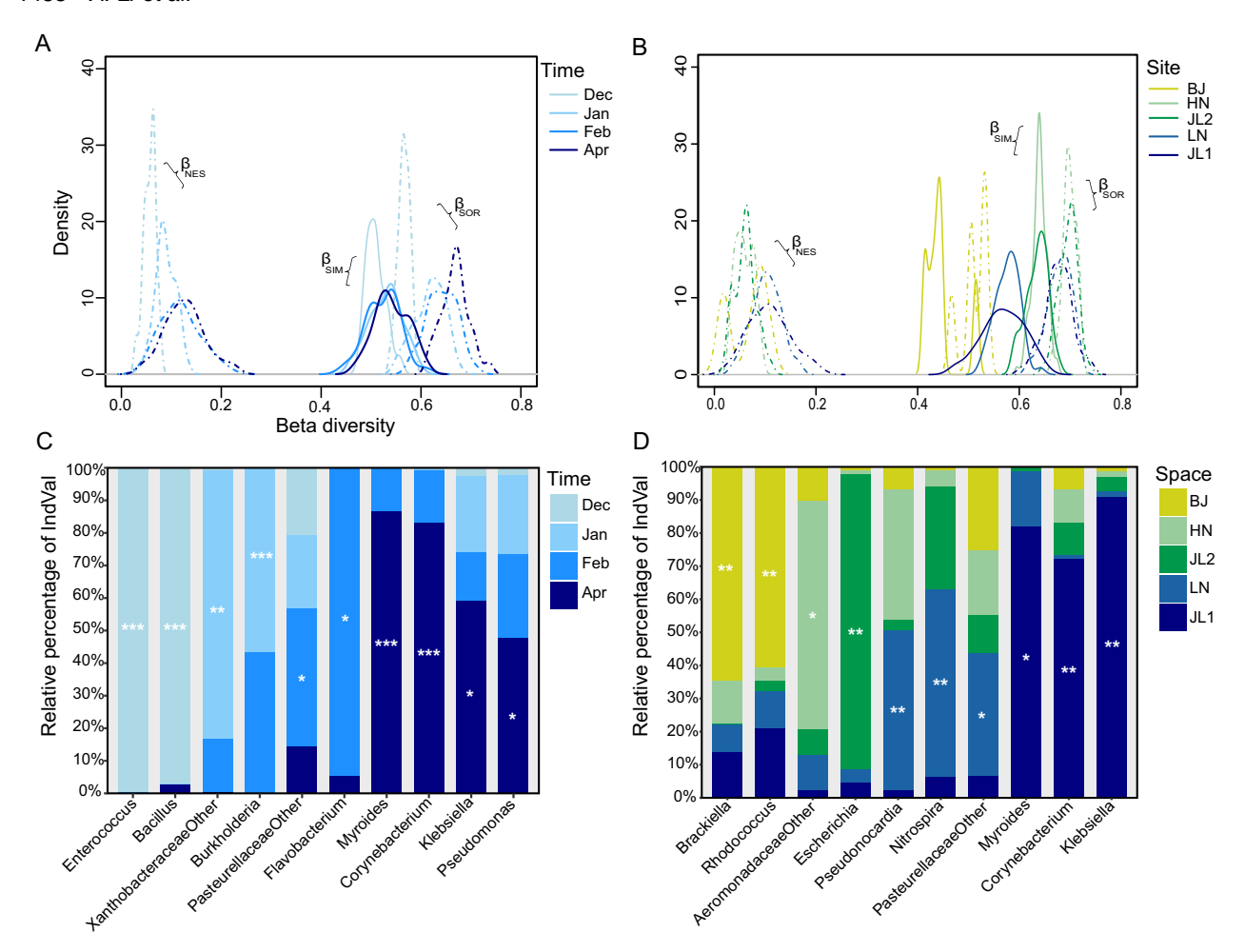


Fig. 3. Partitioning beta diversity and indicator analysis of *R. ferrumequinum* skin bacterial communities through time and space. Temporal (A) and spatial (B) partition of Sørensen Beta-diversity (β_{sor}) into its components β_{sim} (turnover) and β_{nes} (nestedness). Indicator OTUs with relative abundance greater than 1% of four sampling time points (C) and five sites (D). Other represents some OTUs can only be identified at the family level. Stars represent significance indicator OTUs. * P_{adj} < 0.05, ** P_{adj} < 0.01, *** P_{adj} < 0.001.

change of any alpha diversity index (all P > 0.05). Spatial hierarchical clustering showed that samples with closer geographic distances had more similar community structures with the exception of one site (JL1; Fig. S7). A significant positive correlation was also examined between geographic distance and Bray–Curtis dissimilarity among individual pairs of bats (P < 0.001; Fig. 2C), with the closer the geographic distance, the more similar the bacterial communities. A positive trend was observed between bat roosting temperature and Bray–Curtis dissimilarity (P < 0.001; Fig. 2C).

Beta diversity was further partitioned into turnover and nestedness components. Our results revealed that turnover component was disproportionately greater than the nestedness component (Fig. 3A and B), which indicates turnover component contributes the most to overall beta diversity, implying species replacement rather than nestedness driving variation in community structure over

time and space. In addition, 10 indicator OTUs (spanning four phylum and six classes, Fig. 3C) identified were associated with temporal difference in bacterial community structure and 10 indicator OTUs (spanning four phylum and five classes, Fig. 3D) were associated with spatial difference. For example, significant indicators in December were *Enterococcus* and *Bacillus*, but in April indicator taxa were *Myroides*, *Corynebacterium*, *Klebsiella* and *Pseudomonas*.

Relationship between environmental bacteria and skin bacterial communities

We compared the Shannon diversity of bat skin and corresponding environmental samples. Bat skin had a lower Shannon diversity compared to environment for each time point (Mann–Whitney U test, all P < 0.05,

Fig. 1A). While across five sites, bats and their roosting environments showed similar Shannon diversity, except for JL1 (Mann–Whitney U test, all P > 0.05, Fig. 1B). When comparing beta diversity values across all bat skin and environment assemblages together, significant temporal and spatial differences were examined between bat skin and environmental groups based on NMDS of Bray–Cutis dissimilarity (Time: NMDS with stress = 0.17, PER-MANOVA, Pseudo- $F_{1,82} = 14.09$, P = 0.001, $R^2 = 0.15$; Space: NMDS with stress = 0.18, PERMANOVA, Pseudo- $F_{1,83} = 8.40$, P = 0.001, $R^2 = 0.09$; Fig. 4A and B). In addition, there was no difference between the dispersion of variances between bat skin and environmental groups (betadisper; Time: $F_{1,81} = 0.26$, P = 0.60; Space: $F_{1,82} = 0.11$, P = 0.74).

The linear discriminant analysis effect size (LEfse) analysis was used to determine the bacterial OTUs that could explain the difference between these two groups. A total of 522 OTUs were identified to distinguish bat skin and environment classes using the time series data [linear discriminant analysis (LDA) scores > 2, P < 0.05, Table S1]. Among those OTUs with higher relative abundances, 21 and 28 taxa exhibited greater relative abundance in the environment and on bat skin respectively (LDA scores > 4, Table S1; Fig. 4C). We also identified 411 OTUs driving the differences between environmental and bat skin microbiota using the data collected among sites (LDA scores > 2, P < 0.05, Table S2). Twenty-seven taxa associated with bat skin exhibited greater relative abundance compared to the environmental samples, while only nine taxa were more abundant in the environment than on bat skin (LDA scores > 4, Table S2; Fig. 4D).

When examining across all OTUs, we found a positive correlation between bats and their associated environmental sample regardless of time point (Dec.: $\tau = 0.35$, P < 0.001; Jan.: $\tau = 0.22$, P < 0.001; Feb.: $\tau = 0.17$, P < 0.001; Apr.: $\tau = 0.34$, P < 0.001; Fig. 5A). However, when OTUs with relative abundance greater than 0.1% were compared, the relationship between bat skin and environmental samples became significantly negatively correlated (Dec.: $\tau = -0.28$, P < 0.001; Jan.: $\tau = -0.17$, P = 0.031; Feb.: $\tau = -0.29$, P < 0.001; Apr.: $\tau = -0.32$, P < 0.001; Fig. 5A). Across sites including HN, BJ and JL2, the significant negative correlations between bat skin and environmental samples were also detected, except for LN (HN: $\tau = -0.27$, P < 0.001; BJ: $\tau = -0.35$, P < 0.001; JL2: $\tau = -0.15$, P < 0.01; LN: $\tau = -0.05$, P = 0.36; Fig. 5B).

Discussion

Host-associated bacterial communities play an essential role in protecting hosts from pathogens. In this study, we

examined the temporal and spatial dynamics of the skin microbiota of R. ferrumequinum and found that host body condition, bat roosting temperature and geographic distance affected the bacterial community assembly. The enrichment of potentially beneficial bacteria in the skin microbiota may contribute to high resistance of R. ferrumequinum to P. destructans infection.

We found substantial variation in skin bacterial communities over time, which was primarily caused by microbial species replacement in occurrence (Fig. 3A). After controlling for time using partial regression analysis, body condition accounted for the most variation in alpha diversity (Fig. 2), and this observed change may be the adaptation or adjustment of the skin bacterial community as conditions change over the winter. During winter hibernation, bats consume stored fat for energy, which is reflected as a change in body condition. Higher body mass index (BMI) indicates that the host has a better physical condition, which could impact immune response and the ability to cope with environmental stress, which in return influences the ability of bacteria to colonize the skin (Keiser et al., 2016; Hernández-Gómez et al., 2018). This interaction needs to be further characterized experimentally to understand how BMI mediates bacterial colonization.

Our results showed that the bat skin microbiota was not associated with sex, possibly due to the tendency for hibernating bats to cluster in groups, which in turn reduce variation in skin microbiota among individuals. Additionally, population turnover might affect the observed temporal variation of skin bacterial communities since bat individuals were not recaptured and sampled in this study. Actually, tracking individual bats over time was difficult given the large population size. Although this may introduce additional variation, a representative picture of the potential temporal variation in bat skin microbiota is dependable by averaging the data collected by sampling date.

We also found that the skin bacterial communities varied among populations, and that local conditions like bat roosting temperature and geographic distance among sites influenced patterns of bacterial occurrence and distribution. During hibernation, bats lower their body temperatures to near ambient. The change in thermal condition over winter likely has a strong regulating effect on bacteria community structure. Environmental conditions also vary among hibernacula (subterranean sites where bats hibernate during the winter) which influences the community composition, similar to what has been observed in other systems, where environmental temperatures altered skin and gut microbiota (Kohl and Yahn, 2016; Robak and Richards-Zawacki, 2018). Results of the UPGMA and generalized linear models

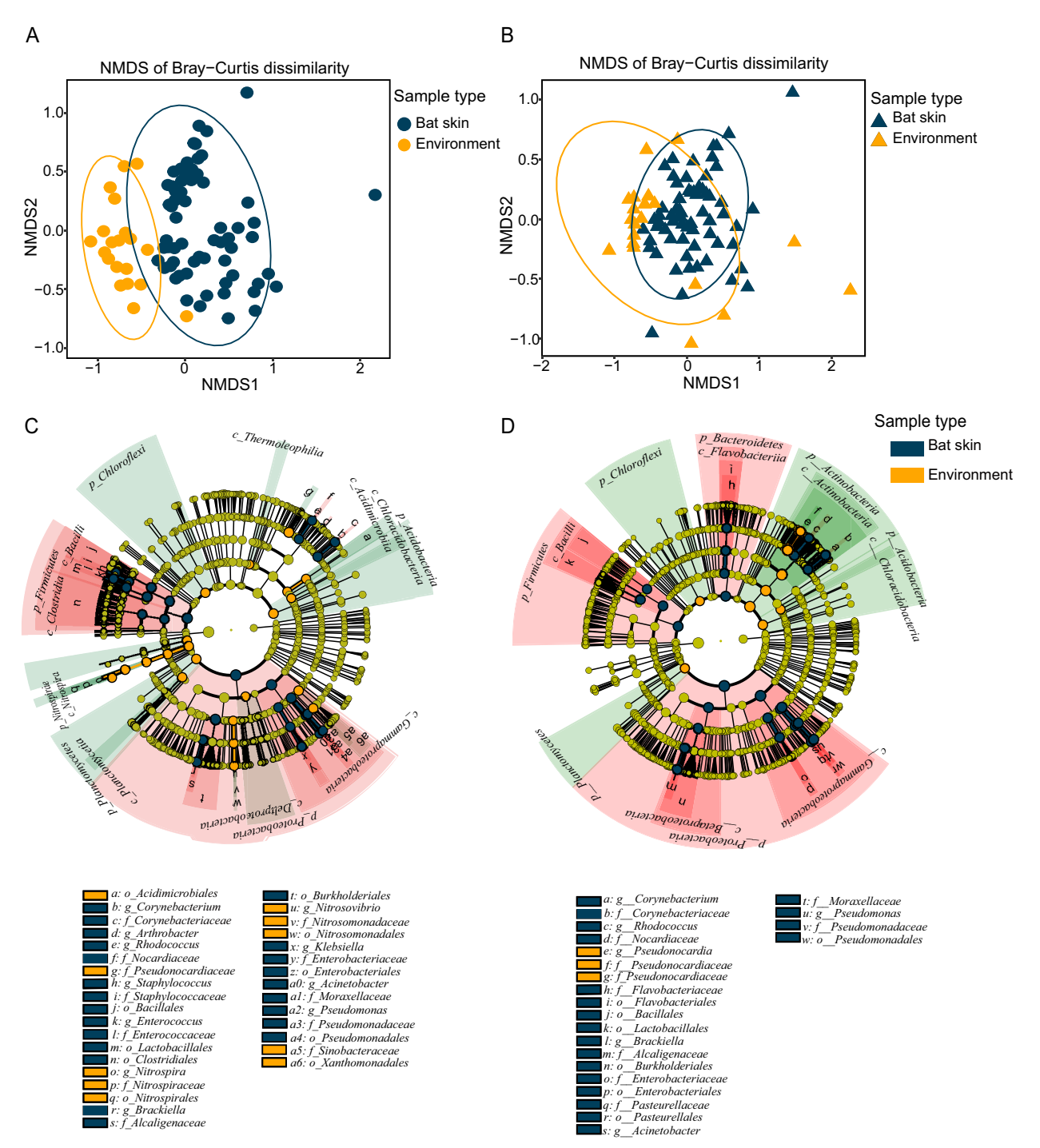


Fig. 4. Differences in bacterial OTUs between bat skin and environmental samples based on nonmetric multidimensional plots and LEfse analysis. Temporal datasets on the left column and spatial datasets on the right. (A) Beta diversity of bat skin and environmental samples from the same population over time and (B) from among populations. NMDS based on Bray–Curtis dissimilarity. Ellipses represent confidence intervals (CI) of 95% for each sample type. (C) Cladogram of OTUs with highest LDA scores (>4) from bat skin and environment using temporal dataset (C) and spatial dataset (D). Different colours represent different groups. Letters represent the position of OTUs in the picture. Red and green colours represent the biomarker in bat skin and environment groups respectively.

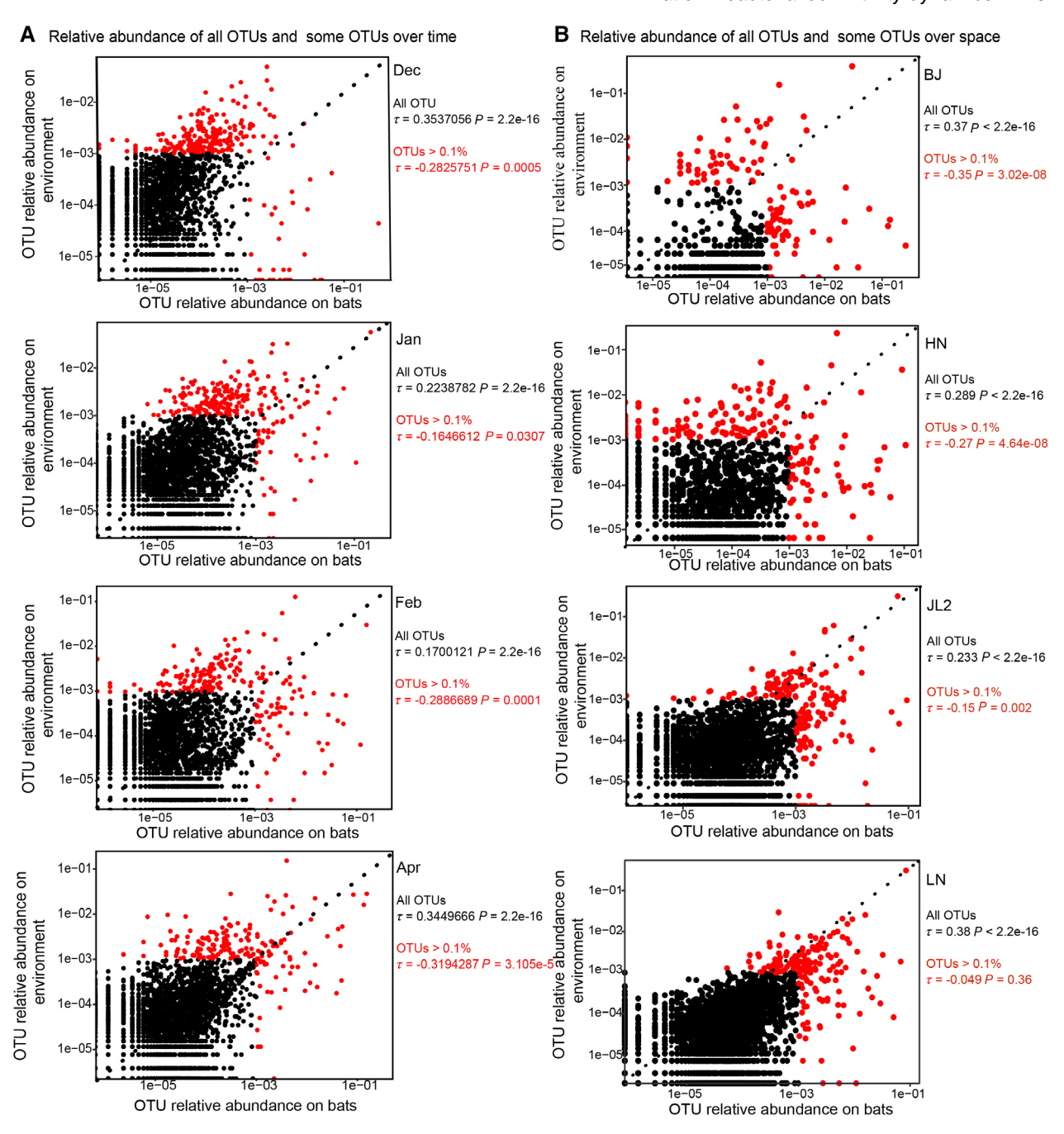


Fig. 5. Relationship between host and corresponding environmental bacteria through time and space. Black dots represent all OTUs, red dots show the OTUs with a relative abundance greater than 0.1%. The right side of the figure shows the correlation coefficient and *P* values. Relative abundance of OTUs of bat skin and corresponding environmental samples at each time point (A) and each site (B).

showed that bacterial communities were more similar between sites that were closer together (Figs 2C and S7), known as the distance-decay relationship by which communities similarity between any two locations decreases as the geographic distance between them increases (Ren et al., 2017). However, other abiotic factors, such as elevation and habitat, could be expected to

be responsible for the microbial variation observed, which could be analyzed in future studies. In general, we found that environmental heterogeneity and dispersal limitation are major factors in determining the spatial variation of skin bacterial communities.

Bacterial community structure has been shown to be influenced by pathogen presence (Jani and Briggs, 2014;

Lemieux-Labonté et al., 2017; Allender et al., 2018; Ange-Stark et al., 2019). However, for this species that shows a high degree of resistance to pathogen infection. we found no difference in the community diversity and structure between infected and uninfected individuals either among or within populations. However, regardless of time or space, indicator analyses revealed that some genera (i.e. Pseudomonas, Rhodococcus, Enterococcus, Bacillus, Corynebacterium) were significantly more abundant in bat skin microbiota (Fig. 3C and D). Those genera have previously been identified on bats and are known for inhibiting the growth of P. destructans in vitro (Cornelison et al., 2014: Micalizzi et al., 2017: Grisnik et al., 2020), and one strain of Pseudomonas fluorescens can reduce disease impacts on bat populations (Hoyt et al., 2019). Moreover, several other genera, reported as antifungal agents in other systems (i.e. Burkholderia, Brackiella, Flavobacterium) (Woodhams et al., 2015), were also identified as the most abundant OTUs of bat skin microbiota. One possible explanation for the high abundance of bacteria with anti-fungal abilities is they may be more suitable for resisting the invasion and growth of P. destructans during hibernation. Bats in Asia have likely coevolved with P. destructans for thousands of years compared to species that are just being exposed to this pathogen for the first time in North America, which may contributes to these differences.

Studies examining influences on host-associated microbiota have shown that shifts in microbes found in the environment can influence host-associated microbiota (Crump and Hobbie, 2005; Shade et al., 2013). while others have found species or population-specific bacterial communities that are influenced very little by the environment (McKenzie et al., 2012). In this study, host skin microbiota showed significant lower alpha diversity than corresponding environment samples at different sampling time points (Fig. 1A), suggesting the microbial difference between host and environment. However, except for one site, no alpha diversity difference between bat skin and the environment was observed at other sites during late hibernation (Fig. 1B), which may be due to different types of environmental conditions affecting the microbial difference among sampling sites. For instance, some organically poor environments (e.g. bare rock surfaces where bats roost) may simply reflect bacterial communities of nearby hosts (Kueneman et al., 2014; Bates et al., 2018).

In addition, we also found that bacterial community structure differed from the community present in the environment. Both the NMDS and hierarchical clustering based on Bray-Curtis dissimilarity revealed that the microbial communities of bat skin and the environment clustered separately with little overlap (Fig. 4 and Figs S4 and S7), indicating that these communities are distinct. In

addition. LEfse revealed that only 15% of OTUs found in the temporal analysis, and 9% of OTUs found in the spatial analysis were descriptive of the difference between host-associated and environmental assemblages. suggesting skin communities on bats host shared the majority of their OTUs with their corresponding environmental. However, the host skin bacterial communities were enriched in bacterial taxa that were low abundances in the environment (red points in Fig. 5), in spite of a significant positive relationship examined for the majority of bacterial taxa between host and environment (black points in Fig. 5). This pattern was consistent with other studies, such as in amphibian, sponge (Webster et al., 2010; Walke et al., 2014; Mariel et al., 2017), suggesting the assembly of skin bacteria is not a complete reflection of the microbiota in the environment. Overall, there is still some degree of interplay between the host and environmental assemblages of bacteria considering the direct exposure of host to the local environment.

In summary, we demonstrated that the skin bacterial community of R. ferrumequinum exhibited temporal and spatial variation during hibernation and was different from environmental microbial reservoirs. More broadly, our results suggest enrichment of multiple taxa with potential antifungal activity may continue resistance to the fungal pathogen over the infectious period. Future research should consider using metagenomics metatranscriptomics to approaches test what function bacterial communities play in resistance to pathogen invasion. A promising strategy to reduce the impacts of P. destructans is the use of probiotic strategies. Considering the dynamics of skin microbiota can help facilitate the development of probiotic bioaugmentation to provide protection for threatened bat species.

Experimental procedures

Field sampling

We collected epidermal swabs from adult *R. fer-rumequinum* with the sealed epiphyseal gaps and environmental swabs from bat roosting locations. Samples were collected at four time points, at approximately 40 days intervals from December 2017 to April 2018 at a cave (JL1) in the Jilin Province, and across four additional populations from Henan Province (HN), Jilin Province (JL2), Liaoning Province (LN) and Beijing (BJ) in March and April 2018. Samples were conducted at those five hibernation sites with a latitudinal gradient and different roosting temperatures for bats where *P. destructans* had been previously found (Hoyt *et al.*, 2020). A total of 63 individual bats were sampled over time from the same population as a temporal dataset and 64 individuals

sampled from different populations as a spatial dataset. In addition, we collected 35 samples from the environment where bats were roosting. Sample sizes for each sampling time point and population were shown in Table 1.

Each individual R. ferrumequinum was removed from the roost with a pair of sterile latex gloves and swabbed using sterile polyester swabs. Two types of epidermal swabs were collected from each individual following the standard protocols to test for P. destructans (Langwig et al., 2014; Hoyt et al., 2016b) and collect skin bacterial communities (Kooser et al., 2015). For P. destructans detection, we sampled bats by dipping sterile polyester swabs in sterile water and then swabbed five times along the forearm and muzzle of each bat. We used a similar method to swab the opposite skin for bacterial community composition but swabbed the entire propatagium and plagiopatagium. Swab tips were stored in individually labelled sterile tubes containing 500 µl of salt preservation buffer (RNAlater®, Tiangen, China) and stored at -20°C within 24 h of sampling and held until DNA extraction. In addition, samples of local environment were also collected by swabbing cave walls under each individual hibernating bat for five times along the walls in linear strokes (approx. 5 cm) and preserved in the same way. Temperature was recorded by using a Fluke 62 MAX IR Thermometer (Fluke, Everett, WA, USA) taken directly next to each sampled bat, which represents bat roosting temperatures (Hoyt et al., 2016a). Swabbing was conducted prior to bats arousing from torpor while their body was still near ambient temperature. After swabbing, we measured and recorded each individual's weight and forearm length to calculate the BMI (BMI = weight/forearm length). All bats were released immediately after sampling. The sampling was performed by the same person in order to prevent individual variation in swabbing technique. All the studies have been approved by the Laboratory Animal Welfare and Ethics Committee of Jilin Agricultural University.

Pseudogymnoascus destructans test

Fungal DNA was extracted from swabs with a modified DNeasy blood and tissue extraction kits (Qiagen, Hilden, Germany). The protocol was modified for fungal extractions to include lyticase during the lysis step in addition to the proteinase K and buffer ATL (Shuey et al., 2014; Hoyt et al., 2016a). Per DNA extraction plate contained eight negative controls (blanks). To determine each individual's infection intensity, we used a real-time quantitative PCR for P. destructans diagnosis developed by Muller et al. (2013). All samples were run in duplicate with the positive control derived from the isolate P. destructans ATCC MYA-4855. To calculate fungal loads, in nanograms, serial dilutions of a quantified standard of the positive control (2 ng μ l⁻¹) were used to generate the equation: Fungal load = $10^{(Ct - 22.04942)/-3.34789}$ (Langwig et al., 2014). All negative controls had no P. destructans detection.

Bacterial DNA extraction and sequencing

Whole genomic DNA was extracted from swabs using the E.Z.N.ATM Mag-Bind Soil DNA Kit (OMEGA Bio-Tek, Norcross, GA, USA) according to the manufacturer's protocol. The samples were transferred to centrifuge tubes containing Buffer SLX Mlus and vortexed at maximum speed to lyse samples. Then we obtained the supernatant through multiple steps of incubation and centrifugation. Finally, tubes were placed on magnetic separation devices suitable to magnetize the Magsi particles and added buffers into tubes according to instructions. After DNA extraction was completed, the first PCR step was performed to amplify the V3-V4 region of the bacteria 16S ribosomal RNA gene with the universal primers 341F and 805R (Eiler et al., 2012). PCR amplifications were performed with a Mastercycler Nexus GSX1 (Eppendorf, Germany) in final volume of 30 µl containing 10 ng of genomic DNA, 15 μ l 2 \times Tag Master Mix, 1 μ l

Table 1. The sample size of skin bacterial community and environmental samples, as well as site information in this study.

Date	Hibernation period	Туре	Site	Sample size (environment)	Roosting temperature (mean \pm SD)	BMI (mean \pm SD)
Dec. 5, 2017	Early	Temporal	Jilin Province (JL1)	9 (5)	8.3 ± 0.39	0.44 ± 0.04
Jan. 17, 2018	Middle	Temporal .	Jilin Province (JL1)	20 (5)	8.02 ± 0.26	$\textbf{0.39} \pm \textbf{0.04}$
Feb. 27, 2018	Middle	Temporal	Jilin Province (JL1)	14 (5)	8.31 ± 0.13	$\textbf{0.35} \pm \textbf{0.04}$
Apr. 8, 2018	Late	Temporal	Jilin Province (JL1)	20 (5)	8.67 ± 0.16	0.31 ± 0.02
Apr. 8, 2018	Late	Spatial	Jilin Province (JL1)	20 (5)	8.67 ± 0.16	0.31 ± 0.02
Mar. 25, 2018	Late	Spatial	Henan Province (HN)	10 (3)	8.19 ± 0.40	$\textbf{0.30} \pm \textbf{0.02}$
Mar. 27, 2018	Late	Spatial	Beijing City (BJ)	4 (4)	10 ± 0.87	$\textbf{0.30} \pm \textbf{0.02}$
Apr. 5, 2018	Late	Spatial	Jilin Province (JL2)	14 (5)	8.07 ± 0.47	$\textbf{0.32} \pm \textbf{0.02}$
Apr. 6, 2018	Late	Spatial Spatial	Liaoning Province (LN)	16 (5)	$\textbf{7.90} \pm \textbf{0.41}$	0.31 ± 0.01

Bar-PCR primer F and 1 ul primer R. The conditions for PCR were as follows: one denaturation step of 94°C for 3 min: with five cycles at 94°C for 30 s. 45°C for 20 s. 65°C for 30 s; 20 cycles of denaturation at 94°C for 20 s, annealing at 55°C for 20 s and extension at 72°C for 30 s. and a final extension at 72°C for 5 min. Another 30 µl reaction mixture contained 20 ng of the first step amplification product, 15 ul 2× Tag master Mix and 1 ul each primer was used for the second PCR step under the following conditions: denaturation at 95°C for 3 min, five cycles of denaturation at 94°C for 20 s, annealing at 55°C for 20 s and extension at 72°C for 30 s, and a final extension at 72°C for 5 min. PCR amplicons were purified with Agencourt AMPure XP (Beckman Coulter, USA) and quantified DNA concentration of each sample using the Qubit 2.0 DNA Assav Kit (Life, USA) to normalize samples prior to Illumina Miseg (2 × 300 bp) sequencing in Sangon Biotech (Shanghai, China).

In this study, the total number of raw sequences generated from different sampling time points (JL1 population) and different sites was 4 971 629 [average 59 899 reads/ sample [range from 41 299 to 88 478)] and 5 044 014 [average 60 048 reads/sample (range from 35 832 to 91 204)] respectively. The adapter sequences added in the process of sequencing were first removed by cutadapt v1.2.1 (Martin, 2011). Forward and reverse reads were formed into contigs using QIIME v1.9.1 pipeline based on the base overlap length of at least 10 bp and no mismatch allowed (Caporaso et al., 2010). Highquality reads were obtained using the following criteria: no presence of ambiguous bases (N), no errors in barcode sequence were allowed, a minimum of five consecutive high-quality base pairs ($Q \ge 20$) and a maximum of three consecutive low-quality base paired were allowed. After quality processing, a total of 4 674 791 (average 56 323 reads/sample) and 4 492 098 reads (average 53 477 reads/sample) were obtained from different sampling time points and sites respectively. Unique sequences were identified and clustered into OTUs at a sequence similarity threshold of 97% based on the UPARSE method, with singletons and chimeric sequences exclude during this process (Edgar, 2013). Taxonomic information was provided for each OTU against the Greengenes database and assigned taxonomy using Ribosomal Database Project Classifier (Wang et al., 2007; McDonald et al., 2012). Furthermore, phylogenetic tree files were also created in the QIME pipeline. To avoid interferences from rare OTUs, which may be errors, the OTUs were removed based on <0.001% of total reads (Bokulich et al., 2013). Finally, to standardize sampling effort across samples, the OTU table was rarefied according to the lowest number of reads, that is, the remaining reads for per sample at temporal and spatial datasets are 32 746 and 26 396 respectively.

Data analysis

To determine the change in skin bacterial community diversity and structure, and what factors were explanatory of variation in assemblage diversity and structure, alpha diversity metrics including Shannon diversity, Observed OTUs and Faith's Phylogenetic Diversity (PD) were calculated separately for samples collected from each time point and each site. These three alpha diversity indices were selected because the Observed OTUs count the number of distinct OTUs in each sample. Shannon diversity considers both community richness and evenness, whereas PD incorporates phylogenetic differences between species (Faith, 1992; Dubois et al., 2017). Non-parametric Kruskal-Wallis tests (since normal distributions of the data or homogeneity of variances were rejected according to Shapiro and Bartlett tests in the package stats respectively) were used to compare alpha diversity through different sampling time points and among different populations respectively. The P-values for multiple comparisons were corrected using Bonferroni correction (Hochberg, 1988). Bray-Curtis dissimilarity matrices were used to calculate the beta diversity and were visualized with NMDS in k = 2 dimensions using the ordinate() and plot_ordination() functions in R package phyloseg (McMurdie and Holmes, 2013). A nonparametric analysis of variance (PERMANOVA) based on 999 permutations was used to test the significance for beta diversity through different sampling time points and among different populations using adonis() function in the package vegan respectively (Oksanen et al., 2018). Post hoc pairwise testing (pairwise differences between groups) was assessed with the pairwise.adonis() function in the package pairwiseAdonis, and Bonferroni correction was applied for multiple comparisons (Arbizu, 2017). The betadisper() function was used to evaluate homogeneity of dispersion among sample groups. We also used PER-MANOVA (999 permutations) to test whether the P. destructans status (positive/negative) or sex affects the skin bacterial community structure. To account nestedness, we stratified by time for different sampling time points, and by site for different populations in PERMANOVAs. In order to determine the relative importance of time versus space to changes in the skin bacterial community, the ANOSIM analysis of the Bray-Curtis dissimilarity was used for statistical analysis and plotted using NMDS (k = 2 dimensions) in the package *vegan*.

To account for the correlation between bat roosting temperature, BMI, fungal loads and time (e.g. BMI decreases, and roosting temperature and fungal loads increase over winter), we used a partial regression approach where we explored how much variation each variable explained after accounting for the effect of one of the others. We regressed observed OTUs, PD and

Shannon diversity over time and used the residuals from that relationship as the response variable in a linear model with BMI, bat roosting temperature and fungal loads. In addition, we examined the effect of geographic distance and bat roosting temperature on Bray-Curtis dissimilarity among individual pairs of bats using a generalized linear mixed model with a beta distribution and a logit link. In this model, log-transformed geographic distance and bat roosting temperature were set as fixed effects, and site was included as a random effect. The pairwise geographic distance between samples was calculated by Geographic Distance Matrix Generator v.1.2.3 based on the coordinates of hibernacula.

An unweighted pair group method with arithmetic mean (UPGMA) was used to evaluate clustering patterns across sampling time points and populations. UPGMA was used on Bray-Curtis dissimilarity of mean OTU relative abundances greater than 0.1% at the genus level and heatmap visualization was completed in the package pheatmap (Kolde, 2015). To reveal the assembly mechanism of bacterial community composition, we computed three multiple-site dissimilarities ($\beta_{sim} + \beta_{nes} = \beta_{sor}$) based on Sørensen dissimilarity indices (presenceabsence data) to account for the turnover (β_{sim} : the replacement of some species by others) and nestedness (β_{nes}) : species loss between samples) components of total beta diversity (β_{sor}) through time and space using beta. multi() function in the package betapart (Baselga, 2010; Baselga et al., 2018). In addition, to identify OTUs most responsible for the temporal and spatial variability in skin bacterial communities on R. ferrumequinum, indicator analysis using the OTUs with relative abundance larger than 1% at genus levels was performed. The indicator value (IndVal) compares the relative abundance distributions of OTU across predefined groups (each sampling time point and site). It provides an index ranges from 0 (indicative of an OTU evenly distributed across all groups) to 1 (indicative of an OTU in one group but not others). All computations of IndVal were done in the package indicspecies accessed by the multipatt() function (Cáceres and Legendre, 2009), and significance was assessed with 9999 permutations. The P-values for multiple comparisons were corrected using the false discovery rate procedure. OTUs with corrected P-values <0.05 and IndVal ≥0.4 were retained as indicators (Lemieux-Labonté et al., 2017). The parameter IndVal.g was used since it corrects for unequal group size.

To address the relationship between host-associated skin bacteria and environmental bacteria, we first calculated the Shannon diversity and compared it by Mann-Whitney *U* test between bat and environmental samples. Beta diversity was calculated and visualized the same as described above. PERMANOVA listing time or site as

'strata' and permutation analysis of multivariate homogeneity of group dispersions with 999 permutations were also used to test significance for beta diversity. In order to determine which OTUs explained the difference in bacterial community structure, we used LEfse method (Segata et al., 2011). According to previous studies (McKenzie et al., 2012), OTUs with LDA scores >2 were considered informative, while the OTUs with LDA scores >4 were chosen for further analysis. In addition, to determine the correlation between host and environmental samples. Kendall's tau according to OTU relative abundance were calculated (Rebollar et al., 2016). These correlations were analyzed using all OTUs or just OTUs with relative abundance greater than 0.1%.

Acknowledgements

This work was supported by the National Natural Science Foundation of China (grant numbers 31961123001, 31770403, 32171525 and 31670390), Jilin Provincial Natural Science Foundation (grant number 20180101272JC), and the Program for Introducing Talents to Universities (B16011) and the US National Science Foundation (DEB-1911853). We thank Yujuan Wang and Zhongwei Yin for their assistance in laboratory work and field sampling, and Xiaobin Huang for his help in data analysis.

Data Availability Statement

All raw sequence data are deposited in the NCBI sequence read archive with the accession numbers SRP255469 and SRP255471 respectively.

References

Allender, M.C., Baker, S., Britton, M., and Kent, A.D. (2018) Snake fungal disease alters skin bacterial and fungal diversity in an endangered rattlesnake. Sci Rep 8: 12147.

Ange-Stark, M., Cheng, T.L., Hoyt, J.R., Langwig, K.E., Parise, K.L., Frick, W.F., et al. (2019) White-nose syndrome restructures bat skin microbiomes. bioRxiv: 614842.

Arbizu, P.M. (2017) pairwiseAdonis: Pairwise multilevel comparison using adonis. R package version 001.

Azarbad, H., Van, G.C., Niklińska, M., Laskowski, R., Röling, W., and Van, S.N. (2016) Resilience of soil microbial communities to metals and additional stressors: DNAbased approaches for assessing "stress-on-stress" responses. Int J Mol Sci 17: 1-20.

Baselga, A. (2010) Partitioning the turnover and nestedness components of beta diversity. Glob Ecol Biogeogr 19:

Baselga, A., Orme, D., Villeger, S., Bortoli, J., Leprieur, F., Logez, M., and Henriques-Silva, R. (2018) betapart: partitioning beta diversity into turnover and nestedness components. R package version 1.5.1. URL https://CRAN.Rproject.org/package=betapart.

- Bates, K.A., Clare, F.C., Hanlon, O.S., Bosch, J., Brookes, L., Hopkins, K., et al. (2018) Amphibian chytridiomycosis outbreak dynamics are linked with host skin bacterial community structure. Nat Commun 9: 693.
- Bokulich, N.A., Subramanian, S., Faith, J.J., Gevers, D., Gordon, J.I., Knight, R., et al. (2013) Quality-filtering vastly improves diversity estimates from Illumina amplicon sequencing. Nat Methods 10: 57–59.
- Byrd, A.L., Belkaid, Y., and Segre, J.A. (2018) The human skin microbiome. *Nat Rev Microbiol* **16**: 143–155.
- Cáceres, M.D., and Legendre, P. (2009) Associations between species and groups of sites: indices and statistical inference. *Ecology* 90: 3566–3574.
- Caporaso, J.G., Kuczynski, J., Stombaugh, J., Bittinger, K., Bushman, F.D., Costello, E.K., *et al.* (2010) QIIME allows analysis of high-throughput community sequencing data. *Nat Methods* **7**: 335–336.
- Cornelison, C.T., Kevin, M.K., Gabriel, K.T., Barlament, C.K., Tucker, T.A., Pierce, G.E., et al. (2014) A preliminary report on the contact-independent antagonism of *Pseudogymnoascus destructans* by *Rhodococcus rhodochrous* strain DAP96253. *BMC Microbiol* **14**: 246.
- Crump, B.C., and Hobbie, J.E. (2005) Synchrony and seasonality in bacterioplankton communities of two temperate rivers. *Limnol Oceanogr* **50**: 1718–1729.
- Drees, K.P., Lorch, J.M., Puechmaille, S.J., Parise, K.L., Wibbelt, G., Hoyt, J.R., et al. (2017) Phylogenetics of a fungal invasion: Origins and widespread dispersal of white-nose syndrome. Mbio 8: e01941-01917.
- Dubois, G., Girard, C., Lapointe, F.O.J., and Shapiro, B.J. (2017) The Inuit gut microbiome is dynamic over time and shaped by traditional foods. *Microbiome* 5: 151.
- Edgar, R.C. (2013) UPARSE: highly accurate OTU sequences from microbial amplicon reads. *Nat Methods* 10: 996–998.
- Eiler, A., Heinrich, F., and Bertilsson, S. (2012) Coherent dynamics and association networks among lake bacterioplankton taxa. *ISME J* **6**: 330–342.
- Faith, D.P. (1992) Conservation evaluation and phylogenetic diversity. *Biol Conserv* 61: 1–10.
- Grice, E.A., and Segre, J.A. (2011) The skin microbiome. Nat Rev Microbiol 9: 244–253.
- Grisnik, M., Bowers, O., Moore, A.J., Jones, B.F., Campbell, J.R., and Walker, D.M. (2020) The cutaneous microbiota of bats has in vitro antifungal activity against the white-nose pathogen. *FEMS Microbiol Ecol* **96**: 2.
- Hernández-Gómez, O., Briggler, J.T., and Williams, R.N. (2018) Influence of immunogenetics, sex and body condition on the cutaneous microbial communities of two giant salamanders. *Mol Ecol* **27**: 1915–1929.
- Hochberg, Y. (1988) A sharper Bonferroni procedure for multiple tests of significance. *Biometrika* **75**: 800–802.
- Hoyt, J.R., Cheng, T.L., Langwig, K.E., Hee, M.M., Frick, W. F., Marm, K.A., and Mark, B.R. (2015) Bacteria isolated from bats inhibit the growth of *Pseudogymnoascus destructans*, the causative agent of white-nose syndrome. *PLoS One* 10: e0121329.
- Hoyt, J.R., Langwig, K.E., Sun, K., Parise, K.L., Li, A., Wang, Y., et al. (2020) Environmental reservoir dynamics predict global infection patterns and population impacts for

- the fungal disease white-nose syndrome. *Proc Natl Acad Sci USA* **117**: 7255–7262.
- Hoyt, J.R., Langwig, K.E., Sun, K.P., Lu, G.J., Parise, K.L., Jiang, T.L., et al. (2016a) Host persistence or extinction from emerging infectious disease: insights from whitenose syndrome in endemic and invading regions. Proc R Soc Lond B Biol Sci 283: 20152861.
- Hoyt, J.R., Langwig, K.E., White, J.P., Kaarakka, H.M., and Kilpatrick, A.M. (2019) Field trial of a probiotic bacteria to protect bats from white-nose syndrome. *Sci Rep* **9**: 9158.
- Hoyt, J.R., Langwig, K.E., White, J.P., Kaarakka, H.M., Redell, J.A., Kurta, A., et al. (2018) Cryptic connections illuminate pathogen transmission within community networks. *Nature* 563: 710–713.
- Hoyt, J.R., Sun, K.P., Parise, K.L., Lu, G., Langwig, K.E., Jiang, T.L., et al. (2016b) Widespread bat white-nose syndrome fungus, Northeastern China. Emerg Infect Dis 22: 140–142.
- Jani, A.J., and Briggs, C.J. (2014) The pathogen *Bat-rachochytrium dendrobatidis* disturbs the frog skin microbiome during a natural epidemic and experimental infection. *Proc Natl Acad Sci USA* **111**: E5049–E5058.
- Jiménez, R.R., and Sommer, S. (2017) The amphibian microbiome: natural range of variation, pathogenic dysbiosis, and role in conservation. *Biodivers Conserv* 26: 763–786.
- Keiser, C.N., Pinter-Wollman, N., Augustine, D.A., Ziemba, M.J., Hao, L., Lawrence, J.G., and Pruitt, J.N. (2016) Individual differences in boldness influence patterns of social interactions and the transmission of cuticular bacteria among group-mates. *Proc R Soc Lond B Biol Sci* 283: 20160457.
- Kohl, K.D., and Yahn, J. (2016) Effects of environmental temperature on the gut microbial communities of tadpoles. *Environ Microbiol* 18: 1561–1565.
- Kolde, R. (2015) pheatmap: Pretty Heatmaps. R package version 1.0. 12. URL https://CRAN.R-project.org/ package=pheatmap.
- Kooser, A., Kimble, J.C., Young, J.M., Buecher, D.C., Valdez, E.W., Porrasalfaro, A., and Northup, D.E. (2015) External microbiota of western United States bats: does it matter where you are from? bioRxiv, 017319.
- Kueneman, J.G., Parfrey, L.W., Woodhams, D.C., Archer, H. M., Knight, R., and McKenzie, V.J. (2014) The amphibian skin-associated microbiome across species, space and life history stages. *Mol Ecol* 23: 1238–1250.
- Langwig, K.E., Frick, W.F., Bried, J.T., Hicks, A.C., Kunz, T. H., and Kilpatrick, A.M. (2012) Sociality, density-dependence and microclimates determine the persistence of populations suffering from a novel fungal disease, white-nose syndrome. *Ecol Lett* 15: 1050–1057.
- Langwig, K.E., Frick, W.F., Hoyt, J.R., Parise, K.L., Drees, K.P., Kunz, T.H., *et al.* (2016) Drivers of variation in species impacts for a multi-host fungal disease of bats. *Philos Trans R Soc Lond B Biol Sci* **371**: 20150456.
- Langwig, K.E., Frick, W.F., Reynolds, R., Parise, K.L., Drees, K.P., Hoyt, J.R., et al. (2014) Host and pathogen ecology drive the seasonal dynamics of a fungal disease, white-nose syndrome. Proc R Soc Lond B Biol Sci 282: 20142335.

- Lemieux-Labonté, V., Simard, A., Willis, C.K.R., and Lapointe, F.J. (2017) Enrichment of beneficial bacteria in the skin microbiota of bats persisting with white-nose syndrome. Microbiome 5: 115.
- Lorch, J.M., Meteyer, C.U., Behr, M.J., Boyles, J.G., and Blehert, D.S. (2011) Experimental infection of bats with Geomyces destructans causes white-nose syndrome. Nature 480: 376-378.
- Loudon, A.H., Woodhams, D.C., Parfrey, L.W., Archer, H., Knight, R., McKenzie, V., and Harris, R.N. (2014) Microbial community dynamics and effect of environmental reservoirs on red-backed salamanders microbial (Plethodon cinereus). ISME J 8: 830-840.
- Mariel, F.L., Rebollar, E.A., Harris, R.N., Vredenburg, V.T., and Jean-Marc, H. (2017) Temporal variation of the skin bacterial community and Batrachochytrium dendrobatidis infection in the terrestrial cryptic frog Philoria loveridgei. Front Microbiol 8: 2535.
- Martin, M. (2011) Cutadapt removes adapter sequences from high-throughput sequencing reads. Embnet J 17: 10-12.
- McDonald, D., Price, M.N., Goodrich, J., Nawrocki, E.P., DeSantis, T.Z., Probst, A., et al. (2012) An improved Greengenes taxonomy with explicit ranks for ecological and evolutionary analyses of bacteria and archaea. ISME J 6: 610-618.
- McKenzie, V.J., Bowers, R.M., Fierer, N., Knight, R., and Lauber, C.L. (2012) Co-habiting amphibian species harbor unique skin bacterial communities in wild populations. ISME J 6: 588-596.
- McMurdie, P.J., and Holmes, S. (2013) phyloseg: An R package for reproducible interactive analysis and graphics of microbiome census data. PLoS One 8: e61217.
- Micalizzi, E.W., Mack, J.N., White, G.P., Avis, T.J., and Smith, M.L. (2017) Microbial inhibitors of the fungus Pseudogymnoascus destructans, the causal agent of white-nose syndrome in bats. PLoS One 12: e0179770.
- Muller, L.K., Lorch, J.M., Lindner, D.L., O'Connor, M., Gargas, A., and Blehert, D.S. (2013) Bat white-nose syndrome: a real-time TagMan polymerase chain reaction test targeting the intergenic spacer region of Geomyces destructans. Mycologia 105: 253-259.
- Oh, J., Byrd, A.L., Park, M., Kong, H.H., and Segre, J.A. (2016) Temporal stability of the human skin microbiome. Cell 165: 854-866.
- Oksanen, J., Blanchet, F.G., Friendly, M., Kindt, R., Legendre, P., McGlinn, D., and Wagner, H. (2018) vegan: Community ecology package. R package version 2.5-6. URL https://CRAN.R-project.org/package=vegan.
- Pantos, O., Bongaerts, P., Dennis, P.G., Tyson, G.W., and Hoegh-Guldberg, O. (2015) Habitat-specific environmental conditions primarily control the microbiomes of the coral Seriatopora hystrix. ISME J 9: 1916-1927.
- Rebollar, E.A., Hughey, M.C., Medina, D., Harris, R.N., and Belden, L.K. (2016) Skin bacterial diversity of Panamanian frogs is associated with host susceptibility and presence of Batrachochytrium dendrobatidis. ISME J 10: 1682-1695
- Rebollar, E.A., Martínez-Ugalde, E., and Orta, A.H. (2020) The amphibian skin microbiome and its protective role against chytridiomycosis. Herpetologica 76: 167-177.

- Ren, T., Boutin, S., Humphries, M.M., Dantzer, B., Gorrell, J. C., Coltman, D.W., et al. (2017) Seasonal, spatial, and maternal effects on gut microbiome in wild red squirrels. Microbiome 5: 163.
- Robak, M.J., and Richards-Zawacki, C.L. (2018) Temperature-dependent effects of cutaneous bacteria on a frog's tolerance of fungal infection. Front Microbiol 9: 410.
- Round, J.L., and Mazmanian, S.K. (2009) The gut microbiota shapes intestinal immune responses during health and disease. Nat Rev Immunol 9: 313-323.
- Segata, N., Abubucker, S., Goll, J., Schubert, A.M., Izard, J., Cantarel, B.L., et al. (2011) Microbial community function and biomarker discovery in the human microbiome. Genome Biol 12: 47.
- Shade, A., Gregory Caporaso, J., Handelsman, J., Knight, R., and Fierer, N. (2013) A meta-analysis of changes in bacterial and archaeal communities with time. ISME J 7: 1493-1506.
- Shuey, M.M., Drees, K.P., Lindner, D.L., Keim, P., and Foster, J.T. (2014) Highly sensitive quantitative PCR for the detection and differentiation of Pseudogymnoascus destructans and other Pseudogymnoascus species. Appl Environ Microbiol 80: 1726-1731.
- Thaiss, C.A., Zmora, N., Levy, M., and Elinav, E. (2016) The microbiome and innate immunity. Nature 535: 65-74.
- Walke, J.B., Becker, M.H., Loftus, S.C., House, L.L., Cormier, G., Jensen, R.V., and Belden, L.K. (2014) Amphibian skin may select for rare environmental microbes. ISME J 8: 2207-2217.
- Walke, J.B., and Belden, L.K. (2016) Harnessing the microbiome to prevent fungal infections: lessons from amphibians. PLoS Pathog 12: e1005796.
- Wang, Q., Garrity, G.M., Tiedje, J.M., and Cole, J.R. (2007) Naïve bayesian classifier for rapid assignment of rRNA sequences into the new bacterial taxonomy. Appl Environ Microbiol 73: 5261-5267.
- Webster, N.S., Taylor, M.W., Behnam, F., Lücker, S., Rattei, T., Whalan, S., et al. (2010) Deep sequencing reveals exceptional diversity and modes of transmission for bacterial sponge symbionts. Environ Microbiol 12: 2070-2082.
- Woodhams, D.C., Alford, R.A., Antwis, R.E., Archer, H., Becker, M.H., Belden, L.K., et al. (2015) Antifungal isolates database of amphibian skin-associated bacteria and function against emerging fungal pathogens. Ecology 96: 595-595.

Supporting Information

Additional Supporting Information may be found in the online version of this article at the publisher's web-site:

- **Fig. S1.** Infection intensity of *P. destructans* in *R.* ferrumequinum across time and space. Infection intensity varied over time (a) and sites (b), measured as Pd_load, on a log10 scale in nanograms.
- Fig. S2. Stacked bar chart of most abundance bacterial phyla through time (a) and space (b).
- Fig. S3. Temporal and spatial variation of alpha diversity of bat skin. (a) Observed OTUs over time. (b) Phylogenetic

Diversity over time. (c) Observed OTUs across five sites. (d) Phylogenetic Diversity across five sites.

Fig. S4. UPGMA and heatmap based on OTUs with relative abundance > 0.1% across bat skin and environmental bacteria over four sampling time-points. Columns are samples and rows are OTUs. The OTUs are displayed at the genus level.

Fig. S5. Box plot of multivariate homogeneity of group dispersions (variances) of *R. ferrumequinum* skin bacterial communities over four sampling time-points. Different letters (a and b) represent statistically significant differences over sampling time-points, as indicated by the Tukey post hoc tests.

Fig. S6. Relationship between Shannon diversity of host skin and body mass index (a) and bat roosting temperature (b) in

four sampling time-points. Dashed lines represent the relationship between factors (BMI and bat roosting temperature) and Shannon diversity is marginal. Gray ribbons show 95% confidence intervals (CI).

Fig. S7. UPGMA and heatmap based on OTUs with relative abundance > 0.1% across bat skin and environmental bacteria across five sites. Columns are samples and rows are OTUs. The OTUs are displayed at the genus level.

Table S1. 522 OTUs were obtained from LEfSe analysis with an LDA score of > 2.0 based on temporal dataset. The red represented OTUs with LDA > 4.

Table S2. 411 OTUs were obtained from LEfSe analysis with an LDA score of > 2.0 based on spatial dataset. The red represented OTUs with LDA > 4.